Supporting Information (SI) for

Delineating roles of Nb^{V} and Zr^{IV} oxoclusters in aqueous phase degradation of phosphonate nerve agent simulants

Tasnim Rahman,[a] Karoly Kozma,[a] Benjamin A. Atterberry,[b,c] Aaron J. Rossini [b,c], May Nyman[a]

[a] *Department of Chemistry; Oregon State University; Corvallis, OR 97331 USA*
[b] *Ames National Laboratory, Division of Material Science and Engineering, Ames, Iowa, USA, 50011*
[c] *Iowa State University, Department of Chemistry, Ames, Iowa, USA, 50011*

Corresponding author: may.nyman@oregonstate.edu

Experimental Section.

Reagents. Hydrous niobium oxide was obtained as a gift from CBMM (Companhia Brasileira de Metalurgia e Mineração). All chemicals used in this study were reagent grade quality and used as received. Tetramethylammonium hydroxide ($[(CH_3)_4N]OH$/TMAOH), Nb_2O_5, LiCl, and CsCl were used for the synthesis of polyoxoniobates solutions i.e. TMA-Nb_6, TMA-Nb_{10}, Li-Nb_{24} and Cs-Nb_{24}. The Zr_4 metal oxo cluster, denoted $ZrOCl_2$ (moiety formula $Zr_4(OH)_8(H_2O)_{16}^{8+}$) was purchased from Millipore Sigma. Nerve agent simulants, DFP (Diisopropyl fluorophosphate) was purchased from Thermo Fischer Scientific, and DMMP (dimethyl methylphosphonate) was purchased from Millipore Sigma.

Hazard: *diisopropyl fluorophosphate (DFP) is an extremely toxic chemical and should be handled appropriately! It must be handled in small quantities with gloves, in the fume hood. Clean up spill immediately.*

Synthesis of Polyoxoniobates (PONbs) and solutions. TMA-(Nb_6), TMA-(Nb_{10}) and Li/Cs-(Nb_{24}) were synthesized as reported by Fullmer et *al*.[37] and Sures et *al*.[38] respectively, details below. SAXS and Raman spectroscopy were used to confirm successful synthesis.

Briefly, $[(CH_3)_4N]_5[H_3Nb_6O_{19}]\cdot 20H_2O$ $[(TMA)_5Nb_6 = Nb_6]$ was synthesized as follows. Tetramethylammonium hydroxide solution (2.8 M,100 mL) was placed in a 150 mL beaker and heated to 90 °C. Hydrous Nb_2O_5 (20 g) was added in small aliquots, allowing complete dissolution before the adding the next aliquot. The transparent solution was then cooled to room temperature and isopropyl alcohol was added to precipitate the final product. To synthesize $[(CH_3)_4N]_6[Nb_{10}O_{28}]\cdot 6\,H_2O$ $[(TMA)_6Nb_{10}{=}Nb_{10}]$, one gram of Nb_6 was added to 10 mL of ethanol resulting in a white suspension. This suspension was loaded into a 23 ml Teflon cup for a Parr Reactor and heated at 140 °C for 18 h. The brown supernatant was discarded and the white powder was washed under vacuum with 50 mL of ethanol and allowed to dry in air. Yield~0.65 grams (87%).

Li-Nb_{24} and Cs-Nb_{24} were synthesized *in situ* as solutions from TMA-Nb_{10}. We dissolved 1.138g of TMA-Nb_{10} in water and then added LiCl or CsCl (amounts in Table S2) into the solution and stirred up to three days to ensure complete conversion to Nb_{24}, which was monitored by Raman spectroscopy and SAXS. The Zr_4 solution was prepared by dissolving $ZrOCl_2$ (**Table S2**) in 5mL Millipore H_2O.

Nerve agent simulant degradation studies. For the degradation studies, DFP (46 µL DFP in 5mL for 50mM and 8.0 µL DFP in 3mL for 20 mM concentration studies) and DMMP (31 µL DMMP in 5mL, 50mM and 11 µL DMMP in 5mL for 20mM concentration studies) were added to obtain a 1:1 ratio of metal

oxo cluster and nerve agent simulants. Both DFP and DMMP solutions were prepared in 10% D_2O for locking and shimming the NMR instrument. Every 6 hours, reaction solutions were examined by SAXS, ^{31}P, and ^{19}F NMR to track DFP and DMMP degradation rates. DFP is converted to diisopropylphosphate (DIIP) and DMMP breaks down to methylphosphonic acid (MP).

After complete conversion of DFP to DIIP, the clusters were precipitated by adding IPA (for the 50 mmolar solutions) in the reaction solution. EDAX and FTIR data were collected on the precipitate. The reaction precipitates were also redissolved in 9:1 H_2O:D_2O solutions and ^{19}F NMR (DFP) and ^{31}P NMR (DFP/DIIP) spectra were collected.

SAXS and Raman. Raman spectra were collected on a Thermo Scientific DXR spectrometer with 780 nm laser source, 400 lines per mm grating, and 50μm slit with 16 scans, 16 seconds each. Small and wide-angle X-ray scattering was collected on an Anton Paar SAXSess with Cu Kα radiation (1.54 Å) and line collimation with a *q*-range of 0.018-2.5 $Å^{-1}$. The instrument is equipped with a 2-dimensional image plate detector with a sample to image plate distance of 26.1 cm. The solutions and the neat water (background) were sealed in a 1.5 mm glass capillary and the data collection time for each sample was 30 minutes. SAXSquant software was used for data collection and initial processing. Igor Pro software(6.8) utilizing Irena macros was used for the data analysis[35]. For simulated scattering curves, SolX software was used[35].

Solution ^{31}P and ^{19}F NMR Spectroscopy. Proton decoupled ^{31}P and ^{19}F NMR data were collected on a Bruker Ascend 11.7 T spectrometer with a 5 mm BBO probe (200 MHz for ^{31}P with 16 scans, and 470 MHz for ^{19}F with 64 scans). Room temperature spectra were collected at 30.0 °C. Chemical shifts are reported in parts per million (δ) and are referenced to external standards 85% H_3PO4 in H_2O (^{31}P) and $CFCl_3$ (^{19}F).

FT-IR. Fourier transform infrared (FTIR) spectra were recorded on a Nicolet iS10 FTIR spectrometer with a secondary Nicolet iZ 10 module purchased from Thermo Fisher Scientific, Inc. The instrument was equipped with a diamond plate for attenuated total reflectance measurements. Spectra were collected in the air for all samples.

SEM-EDAX. Scanning electron microscopy (SEM) and energy-dispersive X-ray spectroscopy (EDX) measurements were performed on a Quanta 600 SEM to extract the compositional information of all the samples.

Solid-State NMR Spectroscopy. Solid-state NMR spectra were acquired on a widebore 9.4 T Bruker Avance III HD or 14.1 T widebore Bruker NEO NMR spectrometers. Samples were packed into 1.3 mm rotors on the benchtop. 9.4 T NMR spectra were acquired with a Bruker 1.3 mm HX NMR probe. 14.1 T NMR spectra were obtained with a triple resonance Phoenix 1.3 mm HXY probe configured in double

resonance HX mode. ^{19}F, ^{31}P and ^{93}Nb chemical shifts were referenced by using the published reference frequencies relative to ^{1}H.[1] ^{1}H NMR spectra were referenced with respect to neat TMS by using adamantane as an external standard (δ_{iso} = 1.82 ppm). ^{93}Nb NMR spectra were acquired with CT-selective ^{93}Nb pulses. The CT-selective ^{93}Nb pulse durations were determined by dividing calibrated ^{13}C pulse widths by a factor 5 (I + ½, for I = 9/2). A QCPMG (quadrupolar Carr-Purcell-Meiboom-Gill) pulse sequence[2] was used acquire the static and magic angle spinning (MAS) ^{93}Nb solid-state NMR spectra of TMA-Nb_{10}. 20 spin echoes (9.4 T) or 40 spin echoes (14.1 T) were acquired with each total spin echo cycle 200 μs in duration, including the π-pulse and ring-down delays. The recycle delay was 0.4 s and the ^{93}Nb π/2 pulses were 0.7 μs in duration at 9.4 T. The recycle delay was 1.0 s and the ^{93}Nb π/2 pulses were 2.3 μs in duration at 14.1 T. π-pulse durations were double the duration of the π/2 pulses. Between 1024 scans and 8192 scans were acquired for each 1D QCPMG NMR spectrum. ^{1}H decoupling was not applied. The CPMG echoes were co-added in the time domain and the resultant single echo was Fourier transformed to recover echo lineshape NMR spectra. A 2D ^{93}Nb→^{1}H NMR spectrum was obtained using the previously published D-RINEPT (dipolar refocused insensitive nuclei enhanced by polarization transfer) pulse sequence,[3] with $SR4^2_1$ dipolar recoupling applied for a total duration 1.92 ms.[4] 80 scans were acquired per t_1-increment, 64 t_1-increments were acquired, with t_1 incremented in steps of 2 ms, corresponding to a 500 kHz spectral width in the indirect dimension. The States-TPPI (time-proportional phase incrementation) method was used to achieve quadrature detection in the indirect dimension.

MAS and static ^{93}Nb solid-state NMR spectra of the solid precipitated from the 50 mM Nb_{10}-DFP solution was obtained with a spin echo pulse sequence because the ^{93}Nb homogenous transverse relaxation time was short (likely less than 2 ms). The recycle delay was 2 s and 2048 scans were acquired at 9.4 T. The CT-selective (central transition) ^{93}Nb pulse was 1.4 μs in duration for the MAS spectrum and 0.5 μs in duration for the static spectrum. The recycle delay was 2 s and 10240 scans were acquired at 14.1 T. The CT-selective ^{93}Nb pulse was 2.3 μs in duration at 14.1 T. MAS ^{31}P and ^{19}F NMR spectra were obtained with a 50 kHz MAS frequency and a 9.4 T magnetic field. A spin echo pulse sequence was used with a 10 s recycle delay and acquisition of 2048 scans. Continuous-wave ^{1}H decoupling with a 25 kHz ^{1}H RF field was applied during signal acquisition. The ^{19}F MAS NMR spectrum was obtained with a double spin echo (DEPTH) pulse sequence to suppress NMR signals from fluorine-containing components of the probe. The recycle delay was 3.64 s and 128 scans were acquired. A ^{19}F saturation recovery experiment was performed and the ^{19}F NMR signal showed a ^{19}F T_1 of 2.8 s. ^{19}F{^{93}Nb} DE-RESPDOR (Double Echo Resonance Echo Saturation Pulse Double Resonance) NMR experiments were performed with the previously described[5] pulse sequence using the $SR4^2_1$ dipolar recoupling sequence. The ^{93}Nb saturation pulses were 30 μs in duration with a 90 kHz RF field. The control ^{19}F{^{93}Nb} DE-RESPDOR signal decayed after ca. 2 ms of

recoupling, limiting the possible recoupling durations that could be used. The recycle delay was 3.64 s and 128 scans were acquired.

Figures and Tables.

Table S1 Literature summary of warfare agent degradation studies.

POMs	MOFs	Metal oxide/metal hydroxides	doped oxides/metal hydroxides
Mo-POMs $PV_2Mo_{10}O_{40}$[6]	Zn_4 –MOF nodes[7]	**Alkaline earths** MgO,[8] CaO[9]	Zr-FeO(OH), $AlO(OH)•ZrO_2$[10]
Nb-POMs Li/K/Cs-Nb_6[11], $GeNb_{12}O_{40}$,[12] $[PNb_{12}(V^VO)_2{\cdot}V^{IV}{}_4O_{40}$, [13] $[SiNb_{12}O_{40}]$, Mg_3Al-LDH[1]-Nb_6[14]	**Zr_6–MOF nodes** NU-1000,[15] UiO-66,[16] MOF-808,[17] UiO-67,[18] OPAA@PCN-128y,[19] PCN-222[20]	**Transition metals** ZnO,[14] Fe_3O_4, Fe/Fe_3O_4,[21] TiO_2,[22] $Zr(OH)_4$,[23] V_2O_5,[24] CeO_2,[25] MnO_2[26]	Al_2O_3-(Fe_2O_3, V_2O_5, CuO,[27]
Other POMs[28]	NH_2-Al-MIL-101,53[29]	**Main group** SiO_2, Al_2O_3[30]	TiO_2-(Zr,[31] Ge, In_2S_3, Mn,[30] ZrO_2, HfO_2, Fe_2O_3,[10] Ag[32]) $BaTiO_3$[33]
-	-	-	ZnO (Ln)[34]

[1] *[LDH=layered double hydroxide $M^{2+}{}_{1-x}M^{3+}{}_x(OH)_2][An^-]_{x/n}{\cdot}zH_2O$; M= Mg^{2+}, Zn^{2+},Ni^{2+}, Al^{3+}, Ga^{3+}, Fe^{3+}, An=anion including chlorides, nitrates, carbonates]*

Table S2 Studied solutions for nerve agent simulant degradation studies.

Metal-oxo cluster	Concentration of cluster (mM)	Additives / precursors	Concentration of nerve agent (mM)	Cluster : nerve agent ratio
TMA-{Nb_6}	50	-	50	1 : 1
TMA-{Nb_6}	5	-	20	1 : 4
TMA-{Nb_{10}}	50	-	50	1 : 1
TMA-{Nb_{10}}	5	-	20	1 : 4
Li-{Nb_{24}}	50	TMA-{Nb_{10}} + LiCl	50	1 : 1
Li-{Nb_{24}}	5	TMA-{Nb_{10}} + LiCl	20	1 : 4
Cs-{Nb_{24}}	50	TMA-{Nb_{10}} + CsCl	50	1 : 1
Cs-{Nb_{24}}	5	TMA-{Nb_{10}} + CsCl	20	1 : 4
{Zr_4}	50	$ZrOCl_2$	50	1 : 1
{Zr_4}	5	$ZrOCl_2$	20	1 : 4
Control experiments:				
-	0	nerve agent in water	20	n. a.
-	0	50 mM CsCl	50	n. a.
-	0	~10 mM HCl (acidic pH)[1]	20	n. a.
-	0	~1 mM CsOH (basic pH)[2]	20	n. a.

[1] *DMMP: pH=2.33 obtained by 9.6 mM HCl; DFP: pH=2.23 obtained by 10.6 mM HCl*
[2] *DMMP: pH=10.73 obtained by 0.8 mM CsOH; DFP: pH=11.75 obtained by 1.33 mM CsOH*

Table S3 Self-buffering pH of metal-oxo cluster (50 mM) solutions with added nerve agent simulant[1]

Cluster	Before reaction	Cluster plus DFP	Redissolved cluster-post DFP reaction	Cluster plus DMMP	Redissolved cluster-post DMMP reaction
TMA-{Nb_6}	11.9	7.2	7.4	8.7	8.9
TMA-{Nb_{10}}	7.1	7.1	6.4	7.1	6.5
Li-{Nb_{24}}	8.4	7.6	6.5	7.8	6.6
Cs-{Nb_{24}}	9.2	7.0	6.9	8.4	8.6
{Zr_4}	1.3	1.1	N/A[2]	N/A[3]	N/A[3]

[1] *See Table S2 for solution preparation conditions*
[2] *Experiment not done*
[3] *Not soluble in water*

Table S4 pH study of the metal oxo cluster (50 mM) - DFP (50 mM) reaction solution.

Degradation period (hours)	pH of (metal oxo cluster and DFP) reaction solutions				
	{Nb_6}	{Nb_{10}}	Li-{Nb_{24}}	Cs-{Nb_{24}}	{Zr_4}
0	9.5	7.1	8.4	9.2	1.3
6	7.2	7.1	8.0	8.6	1.1
12	7.2	7.1	7.9	7.0	1.1
18	7.2	7.1	7.6	7.0	1.1
24	7.2	7.1	7.6	7.0	1.1
30	7.2	-	7.6	7.0	1.2
36	7.2	-	7.6	7.0	1.1
42	7.2	-	-	7.0	1.1
48	-	-	-	7.0	-

Note: pH measurements were taken until DFP degradation was completed

Table S5 pH aging study of the metal oxo cluster (5 mM) – DFP (20 mM) reaction solution.

System	pH - before DFP added	pH – two hours reaction solution	pH – complete degradation
{Nb_6}	10.0	7.6	n. a. (precipitation)
{Nb_{10}}	7.0	5.6	n. a. (precipitation)
Li-{Nb_{24}}	8.9	8.7	5.1
Cs-{Nb_{24}}	9.1	8.8	n. a. (precipitation)
{Zr_4}	2.2	2.3	n. a. (precipitation)
Control experiments:			
20 mM DFP	n. a.	4.5	2.3 (1 week); 1.2 (2 weeks)

HCl	2.23	2.33	1.12 (1 week)
CsOH	11.8	7.1	1.5 (1 week)

Table S6 Amount of F and P associated with metal-oxo clusters after DFP degradation determined by EDX. [1]

Studied system	**at% metal**	**at% F**	**at% P**	**{$M_{cluster}$} : F : P ratio**
{Nb_6} (50 mM)	92	8	-	1 : 0.5 : 0
{Nb_6} (5 mM)	60	22	4	1 : 2.3 : 0.4
{Nb_{10}} (50 mM)	92	8	-	1 : 0.9 : 0
{Nb_{10}} (5 mM)	80	14	6	1 : 1.8 : 0.7
Li-{Nb_{24}} (50 mM)	87	13	-	1 : 3.6 : 0
Li-{Nb_{24}} (5 mM)	81	14	5	1 : 4.1 : 1.6
Cs-{Nb_{24}} (50 mM)	62	7	-	1 : 2.7 : 0
Cs-{Nb_{24}} (5 mM)	57	7	4	1 : 2.9 : 1.5
{Zr_4} (50 mM)	24	30	46 [2]	1 : 5 : 7.7
{Zr_4} (5 mM)	63	30	- [2]	1 : 2.9

[1] *approximated by EDX, analysis does not include oxygen*
[2] *Zr and P peaks overlap in EDX*

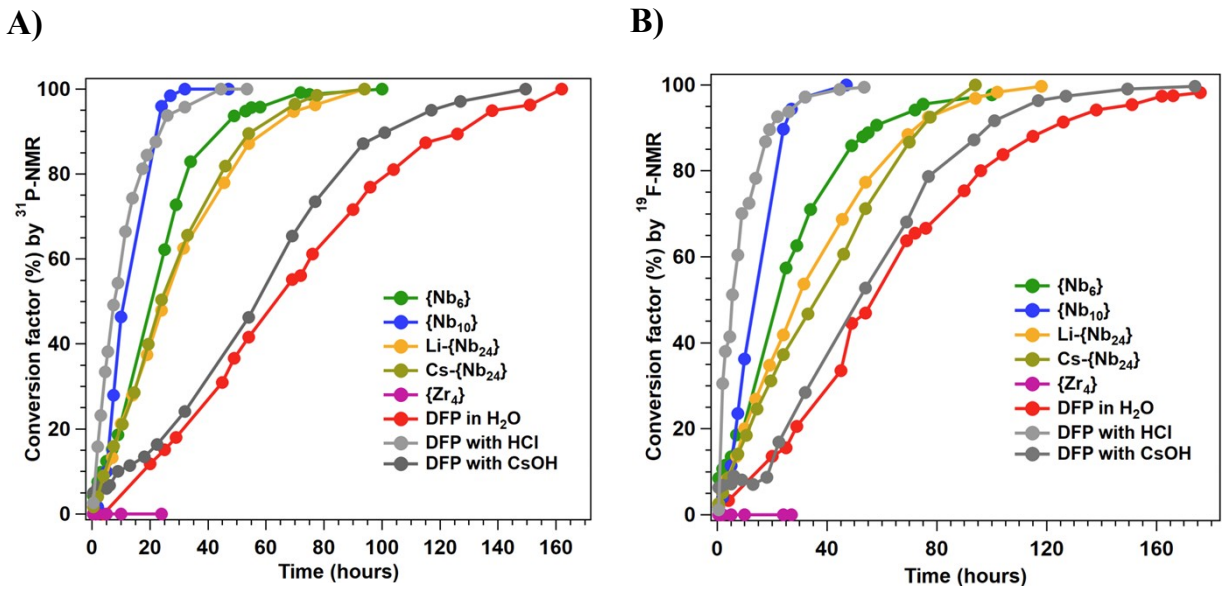

Figure S1 Comparison of DFP degradation rates with the investigated metal-oxo clusters in the 5 mM-20 mM cluster-nerve agent reaction solutions obtained by A) ^{31}P NMR results and B) ^{19}F NMR results. The results exhibit the same general trends.

Table S7 Degradation periods for complete conversion of DFP (20 mM) in the investigated metal-oxo cluster (5 mM) reaction solutions.

System	Conversion (%) by ^{31}P NMR	Degradation period (^{31}P NMR)	Conversion (%) by ^{19}F NMR	Degradation period (^{19}F NMR)
{Nb$_6$}	98.7	3.1 days (75 hours)	97.7	4.2 days (100 hours)
{Nb$_{10}$}	98.4	1.1 day (27 hours)	97.2	1.4 days (32 hours)
Li-{Nb$_{24}$}	96.2	3.2 days (77 hours)	99.6	4.9 days (118 hours)
Cs-{Nb$_{24}$}	98.5	3.2 days (77.5 hours)	100	3.9 days (94 hours)
{Zr$_4$}	n. a.[1]	n. a. [1]	n. a. [1]	n. a. [1]
H$_2$O	96.2	6.3 days (151 hours)	98.2	7.3 days (176 hours)
HCl	100	1.9 days (44.5 hours)	99.5	2.2 days (53 hours)
CsOH	97.0	5.3 days (127 hours)	98.2	7.3 days (176 hours)

[1]precipitated

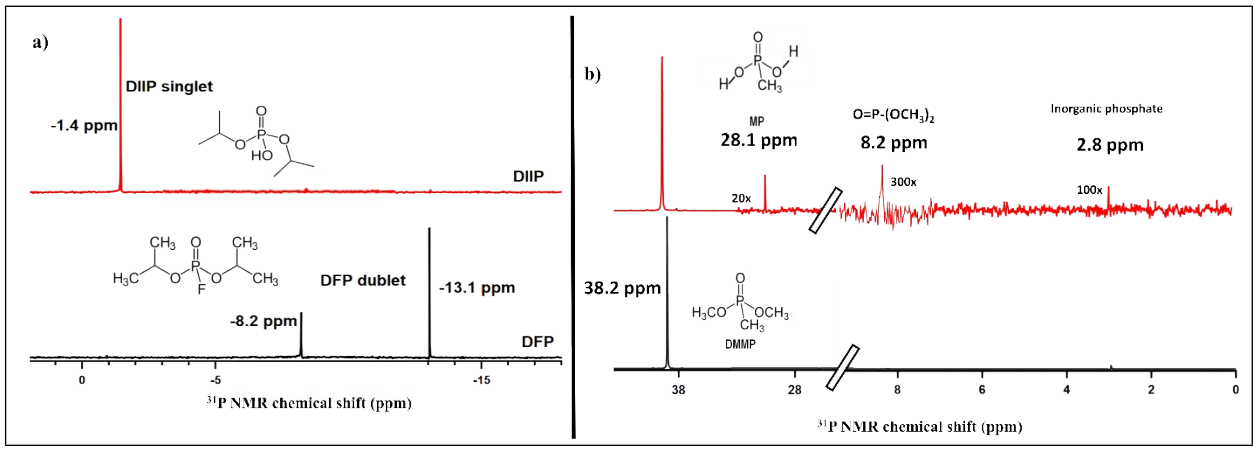

Figure S2 ^{31}P NMR shift a) DFP to DIIP[35]; b) DMMP to MPA[36], for 50 mmolar DFP-50 mmolar cluster solutions.

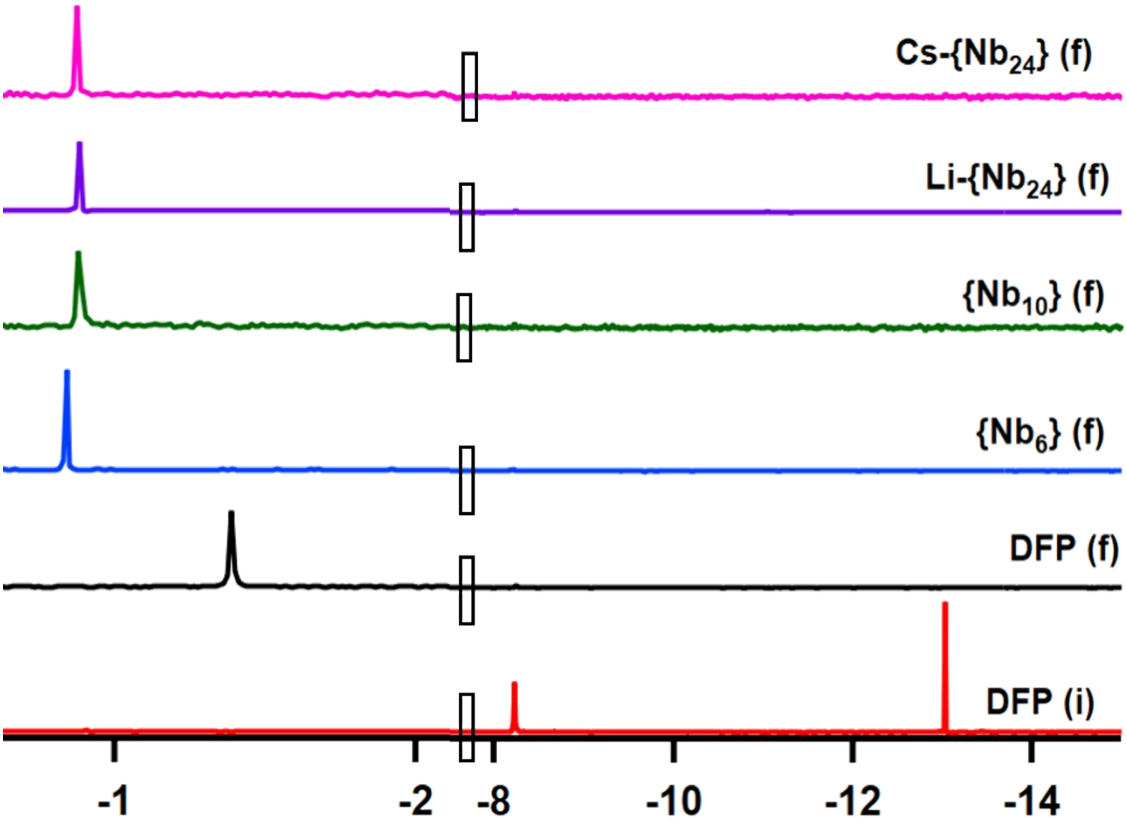

Figure S3 ^{31}P NMR spectra of 50 mM polyoxoniobate - DFP reaction solutions after complete degradation. (i = initial; f = final)

Table S8 ^{31}P chemical shift values of DFP reaction solutions.

Solution composition	^{31}P chemical shift (ppm)	Degradation period (hours)
$\{Nb_6\}$ (50 mM)	-0.86	42
$\{Nb_6\}$ (5 mM)	-0.89	75
$\{Nb_{10}\}$ (50 mM)	-0.86	24
$\{Nb_{10}\}$ (5 mM)	-0.88	27
Li-$\{Nb_{24}\}$ (50 mM)	-0.86	36
Li-$\{Nb_{24}\}$ (5 mM)	-0.89	77
Cs-$\{Nb_{24}\}$ (50 mM)	-0.86	48
Cs-$\{Nb_{24}\}$ (5 mM)	-0.88	77.5
$\{Zr_4\}$ (50 mM)	-1.64	42
$\{Zr_4\}$ (5 mM)	-[1]	n. a.[1]
Control experiments:		
H_2O	-0.93	151
CsCl	-1.44	90
HCl	-1.37	44.5
CsOH	-0.88	127

[1]precipitated

Table S9 ^{19}F NMR chemical shift comparison of metal oxo cluster and DFP (50mM – 50 mM) reaction and redissolved solution.

Metal oxo cluster	Reaction solution (ppm)	Redissolved precipitate (ppm)	Comments
$\{Nb_6\}$ (50 mM)	-120	-117	
$\{Nb_6\}$ (5 mM)	-119.6	-119.7	
$\{Nb_{10}\}$ (50 mM)	-120	-120	
$\{Nb_{10}\}$ (5 mM)	-119.7	-120.2	Free F^- ion
Li-$\{Nb_{24}\}$ (50 mM)	-120	-120	
Li-$\{Nb_{24}\}$ (5 mM)	-120.1	-119.8	
Cs-$\{Nb_{24}\}$ (50 mM)	-120	-119	
Cs-$\{Nb_{24}\}$ (5 mM)	-119.4	-119.6	
$\{Zr_4\}$ (50 mM)	-113.9 (doublet)	not soluble	associated F^- ion[36]
$\{Zr_4\}$ (5 mM)	n. a.	-	
Control experiments:			
H_2O	-146.3	-129.6 (end of reaction)	
HCl	-159.9	-129.6 (end of reaction)	
CsOH	-122.4	-129.5 (end of reaction)	

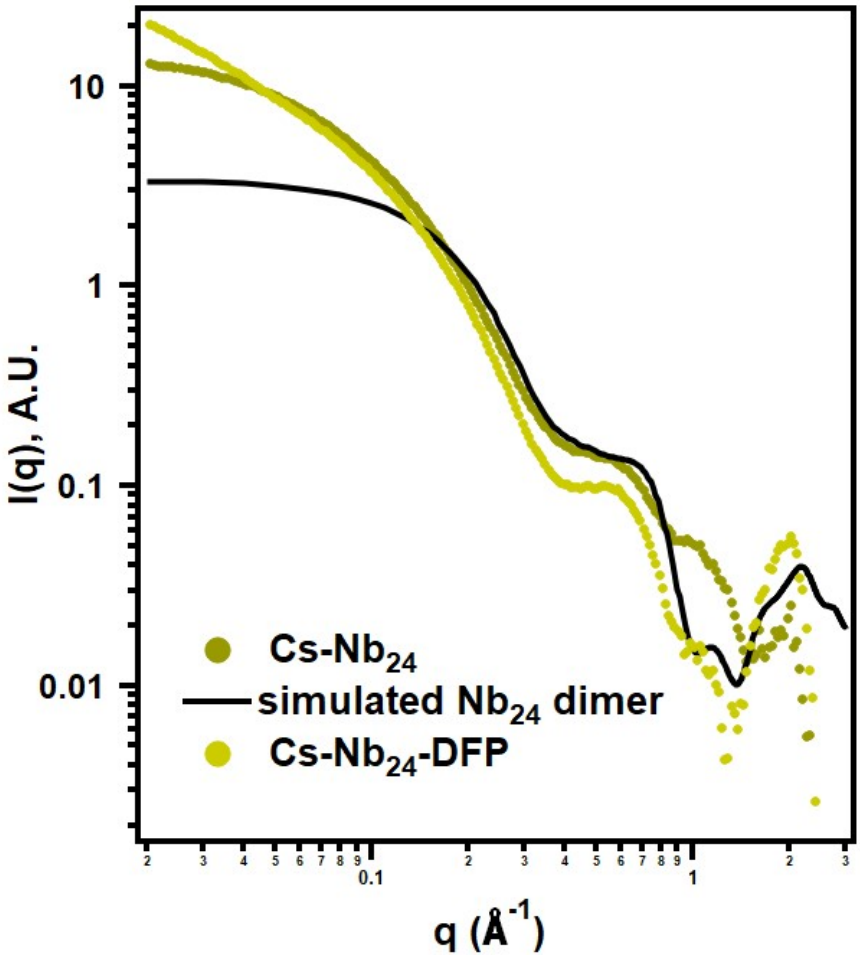

Figure S4 SAXS of Cs-Nb_{24} solution, with and without DFP, compared to simulated Nb_{24} tetramer (see also figure 2 and related discussion).

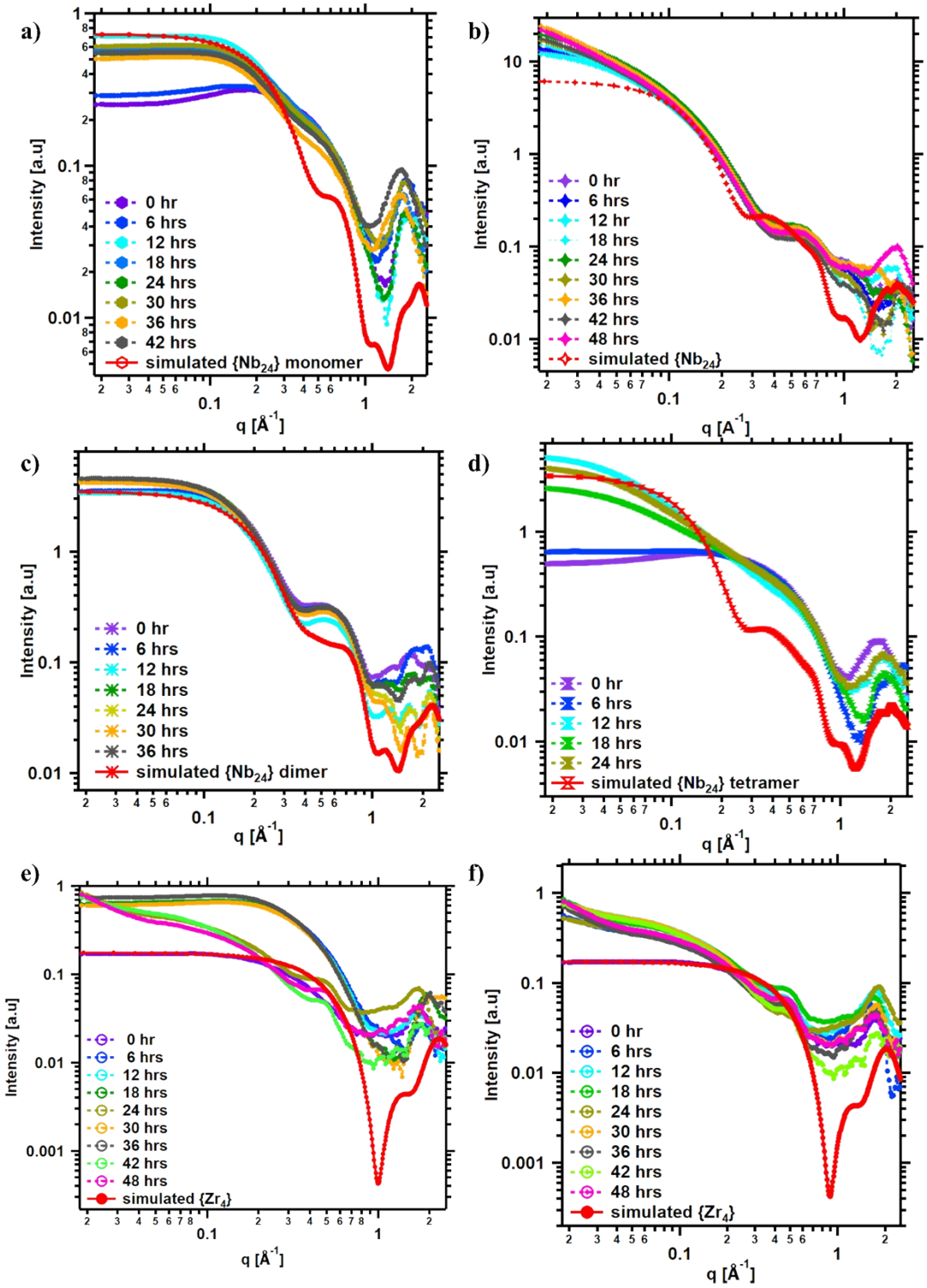

Figure S5 SAXS aging study on DFP reaction solution with a) {Nb_{10}}; b) Cs-{Nb_{24}}; c) Li-{Nb_{24}}; d) {Nb_6}; e) {Zr_4} without DFP and f) Zr_4 with DFP.

Table S10. Parameters for fitting form and structure[35] factors for 50 mM Nb-POM solution SAXS that exhibit structure factors

Nb-POM	Radius[1] (err) Å	Eta[2]	Phi[3] (Å)	Figure for data fit
Nb_6	3.3 (0.3)	0.36	29	S7
Nb_{10}	4.1 (0.4)	0.37	30	S8
Li-Nb_{24}	11.3 (1.6)	0.30	40	S9

[1]spherical form factor
[2]Eta is a unitless value number of nearest neighbors of scattering species
[3]Phi is the distance between scattering species

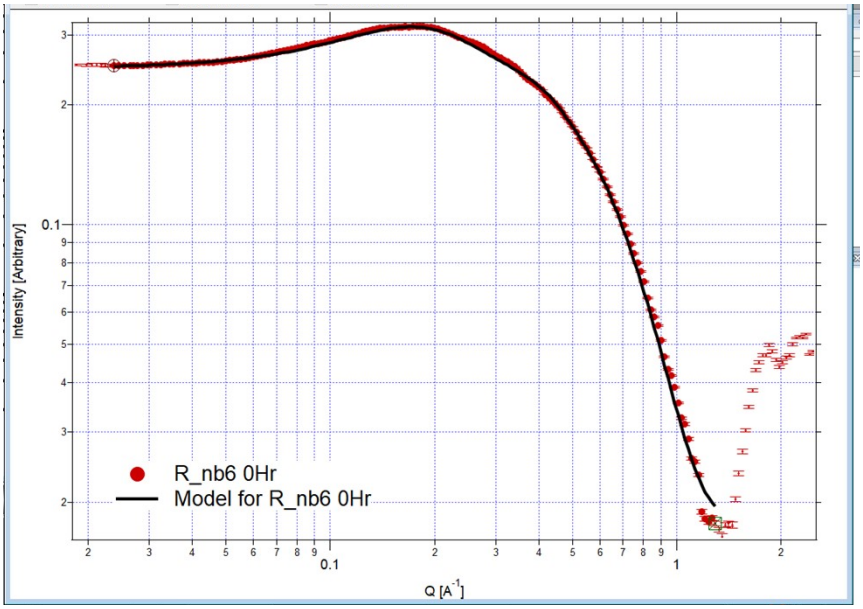

Figure S6. Modeling form and structure factor for 50mM Nb_6 solution.

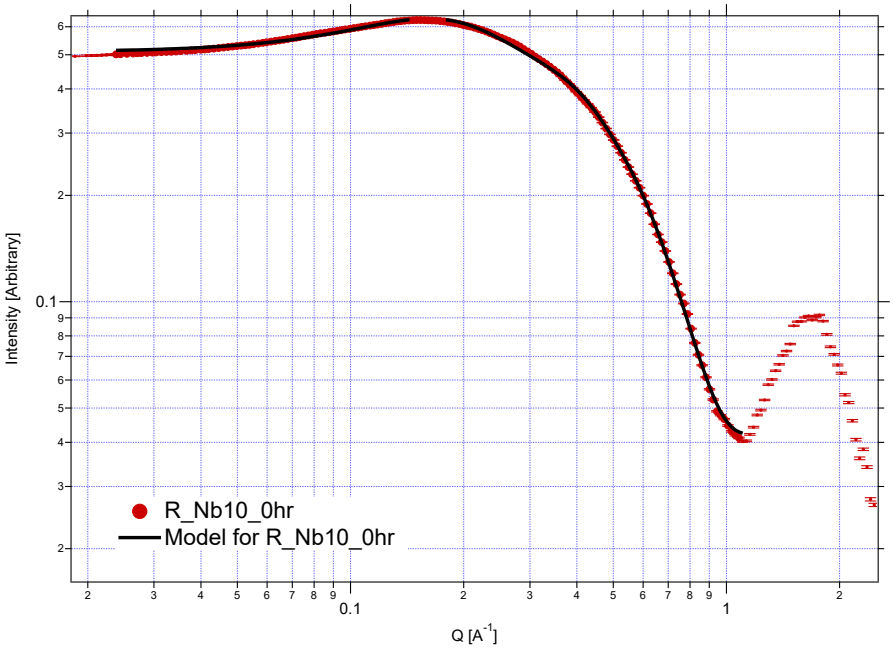

Figure S7. Modeling form and structure factor for 50mM Nb_{10} solution.

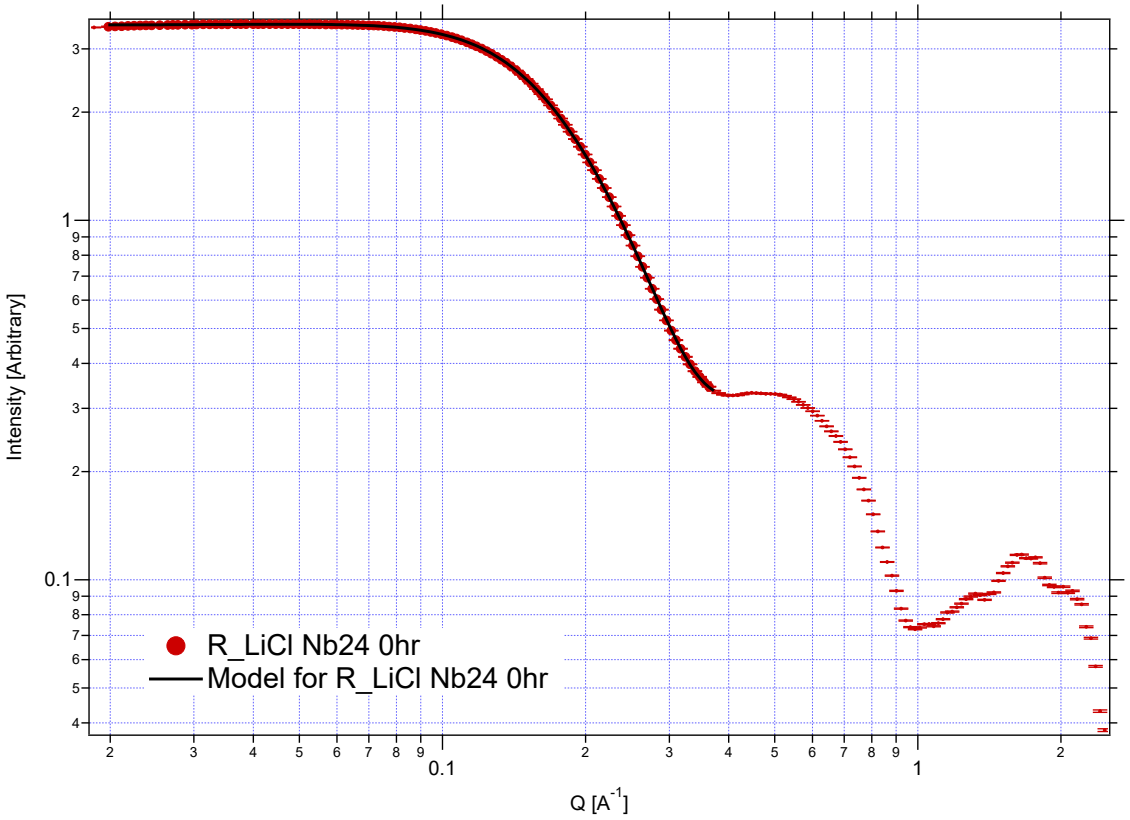

Figure S8. Modeling form and structure factor for 50 mM Li-Nb_{24} solution.

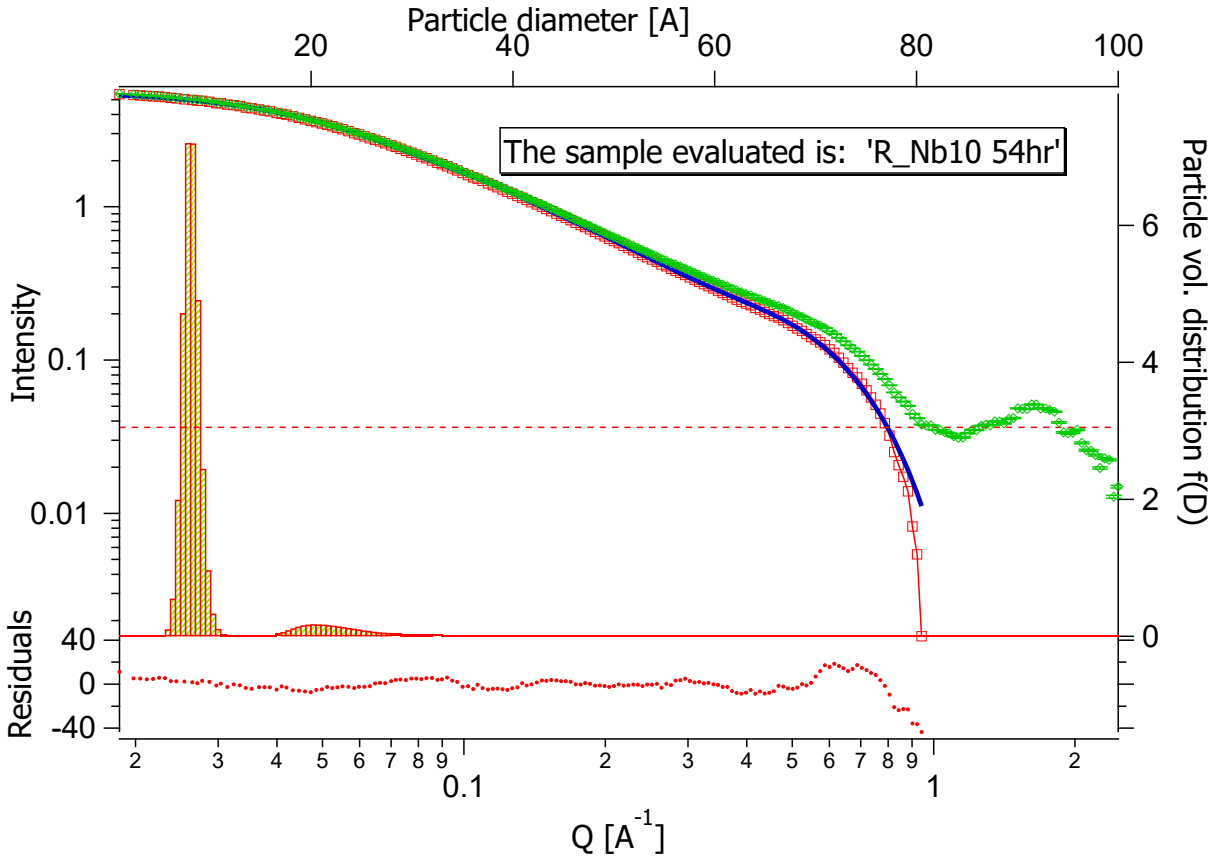

Figure S9. Size distribution analysis of 50 mM Nb_{10} after DPF degradation showing sizes consistent with Nb_7 (major species) and Nb_{24} (minor species).

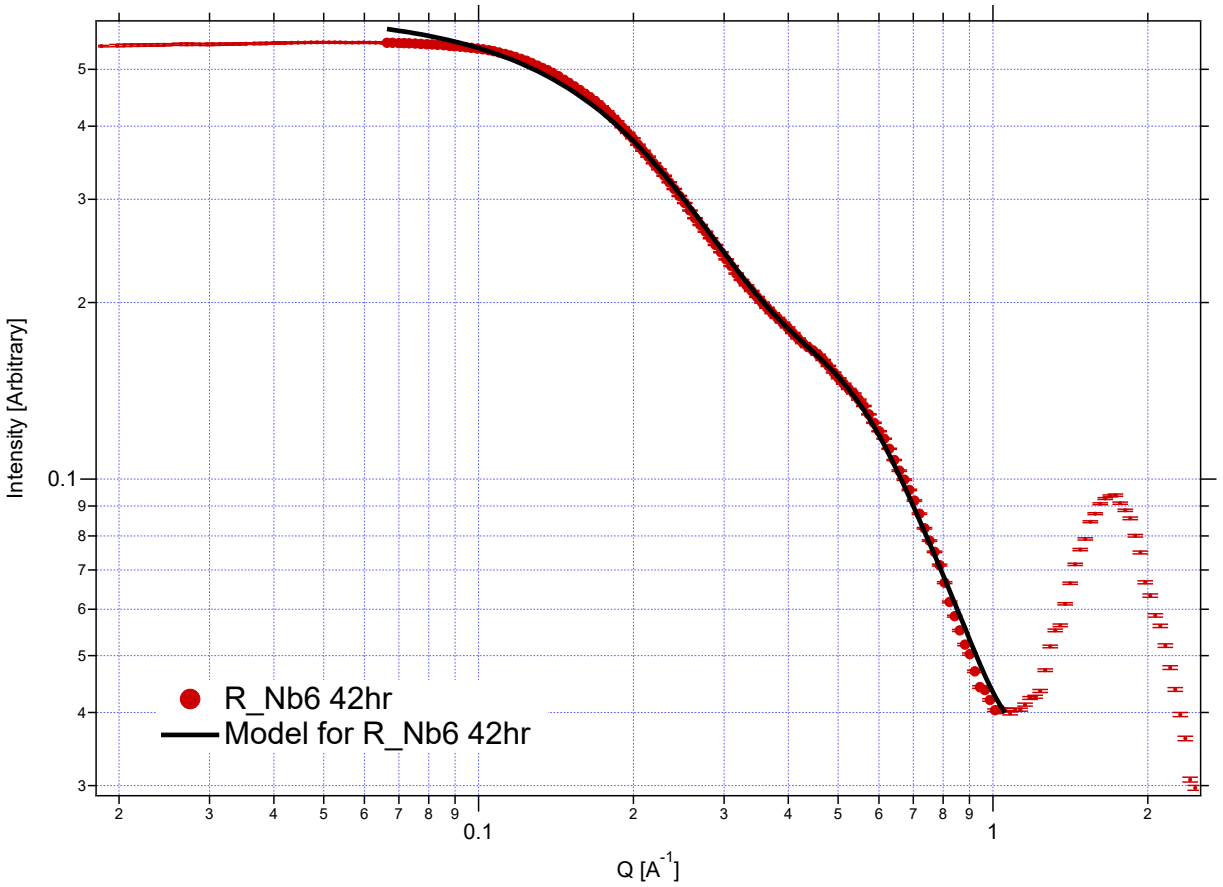

Figure S10. Two phase fit of 50mM Nb_6 following DFP degradation. Phase 1 is consistent with Nb_6: radius=3.7 Å, 94%. Phase 2 is consistent with Nb_{24}: radius=10.5 Å, 6%.

Table S10 Cluster size comparison of metal oxo cluster and DFP reaction and redissolved solution from 50 mM concentration systems.

Metal oxo cluster	**Size and structure of largest metal oxo clusters present**	
	Reaction solution	**Redissolved solution**
{Nb_6}	Nb_{24} monomer	Nb_{24} monomer
{Nb_{10}}	Nb_{24} tetramer	Nb_{24} tetramer
Li-{Nb_{24}}	Nb_{24} dimer	Nb_{24} tetramer
Cs-{Nb_{24}}	Nb_{24} tetramer	Nb_{24} tetramer

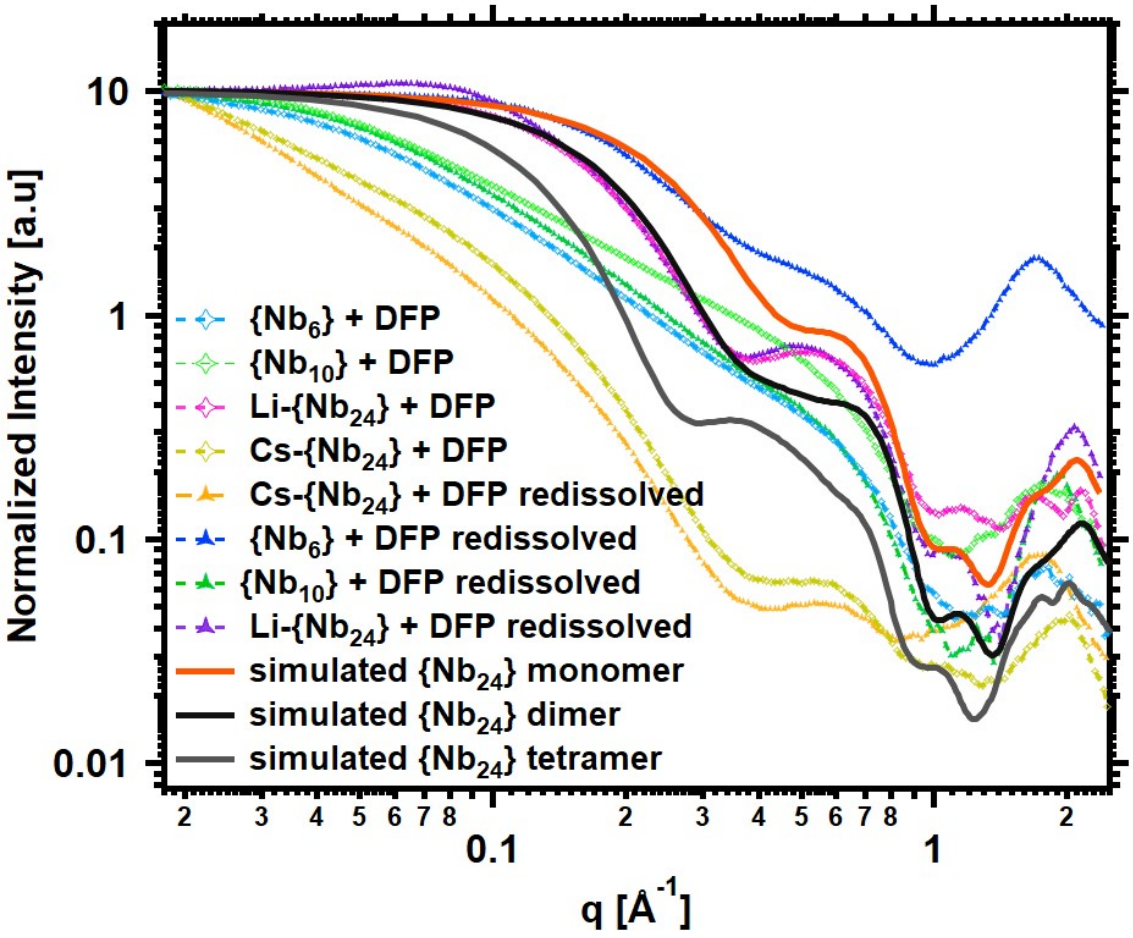

Figure S11 SAXS comparison of metal oxo cluster and DFP reaction (50 mM – 50 mM) and redissolved solutions.

Solid-state NMR analysis of TMA-Nb_{10} and Nb_{10}-DFP (50mM) precipitates

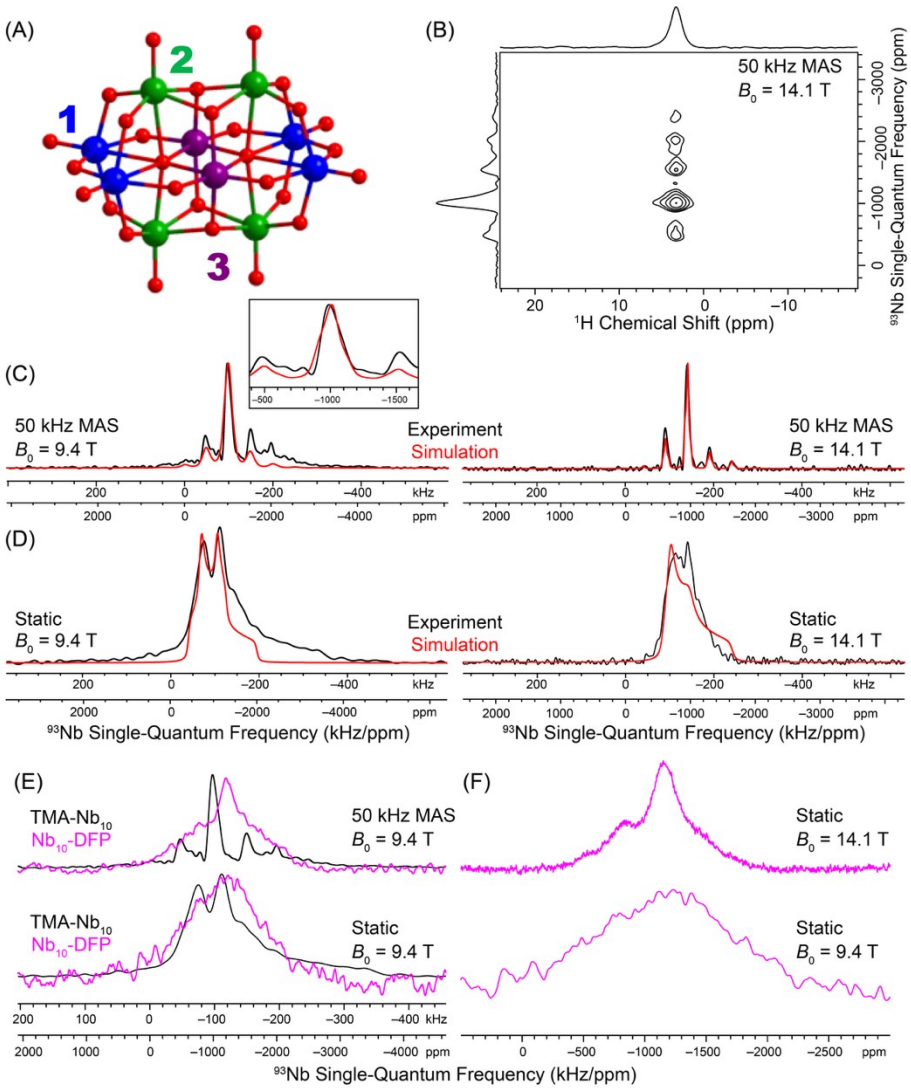

Figure S12. ^{93}Nb solid-state NMR spectra of TMA-Nb_{10} and the Nb_{10}-DFP precipitate collected after reaction. (A) Structural model of TMA-Nb_{10} showing the three different octahedral Nb sites. (B) ^{93}Nb→^{1}H D-RINEPT (dipolar refocused insensitive nuclei enhanced by polarization transfer) 2D spectrum showing the correlation of TMA ^{1}H NMR signals to ^{93}Nb MAS NMR signals. ^{93}Nb solid-state NMR spectra acquired with a QCPMG pulse sequences from samples undergoing (C) MAS with a frequency of 50 kHz, or (D) from stationary (static) samples. NMR spectra were obtained with B_0 = 9.4 T or B_0 = 14.1 T. The inset in (C) shows an expanded view of the isotropic peak. Analytical simulations are shown as red traces overlaid on the experimental NMR spectrum. The simulations used an isotropic chemical shift (δ_{iso}) of –900 ppm, a quadrupolar coupling constant (C_Q) of 26.0 MHz, an EFG tensor asymmetry parameter of 0.95, the span (Ω) of the CS tensor of 825 ppm, and a skew of the CS tensor (κ) of –0.6, and the Euler angle (β) was set to 30°. (E) Comparison of the experimental 9.4 T static and 50 kHz MAS NMR solid-state spectra of TMA-Nb_{10} (black traces) and the precipitate from the 50 mM Nb_{10}-DFP solution (pink traces). (F) Comparison of static ^{93}Nb spin echo NMR spectra of Nb_{10}-DFP precipitate. Spectra are shown for 9.4 T and 14.1 T.

Further details of ^{93}Nb Solid-State NMR Spectra of TMA-Nb_{10} and DFP-Nb_{10}

^{93}Nb solid-state NMR spectroscopy has been extensively used to study niobium oxide materials.[36] We first obtained ^{93}Nb solid-state NMR spectra of TMA-Nb_{10} because the structure of this compound is known. We obtained the ^{93}Nb solid-state NMR spectra at two magnetic fields to understand how the quadrupolar interaction and chemical shift anisotropy (CSA) broaden the ^{93}Nb NMR spectrum. The crystal structure of TMA-Nb_{10} is known and illustrated in **figure S13A**. There are three crystallographically unique Nb sites. However, all Nb atoms reside in distorted octahedral coordination environments. The MAS ^{93}Nb solid-state NMR spectrum of TMA-Nb_{10} shows a single intense broad isotropic powder pattern that is flanked by weaker spinning sidebands (**Figure S12C**). Finally, we also obtained a ^{93}Nb→^{1}H D-RINEPT 2D spectrum that correlates the TMA ^{1}H NMR signals to the ^{93}Nb MAS NMR spectrum. This 2D spectrum confirms that the observed ^{93}Nb NMR signals arise from ^{93}Nb atoms that are within a few Å (dipolar coupled) to the TMA ^{1}H atoms. The static NMR spectra show broad powder patterns (**Figure S12D**).

We simulated the ^{93}Nb NMR spectrum using a single site, with an isotropic chemical shift (δ_{iso}) of –900 ppm, a quadrupolar coupling constant (C_Q) of 26.0 MHz, an EFG tensor asymmetry parameter of 0.95, the span (Ω) of the CS tensor of 825 ppm, and a skew of the CS tensor (κ) of –0.6, and the Euler angle β that describes the relative orientations of V_{33} and δ_{33} was set to 30°. The simulations required the addition of ^{93}Nb chemical shift anisotropy (CSA) to obtain reasonable fits; if ^{93}Nb CSA was excluded, then the sidebands in the MAS SSNMR spectra were too low intensity and the widths of the simulated static ^{93}Nb SSNMR spectra were too narrow. The fitted values of C_Q and Ω are typical of those previously reported for 6-coordinate Nb sites in various oxide materials.[36] The simulations show some clear disagreement with the some of the features seen in the experimental NMR spectra. Therefore, the fitted parameters should only be treated as estimates with significant uncertainty. It is likely that there are multiple overlapping ^{93}Nb NMR signals from the 3 different sites in TMA-Nb_{10} and all sites have somewhat similar ^{93}Nb EFG tensor and CS tensor parameters. In addition, the 9.4 T NMR spectra show additional signal intensity at lower frequencies that could arise from secondary phases or possibly sites with larger C_Q. At 9.4 T, MAS only narrows the right portion of the spectrum, suggesting that the right side of the pattern arises from species with a C_Q of ca. 30 MHz or less. Comparing the ^{93}Nb NMR spectra of the precipitate obtained with a 9.4 T and 14.1 T shows that there is narrowing of the NMR signal at higher field, suggesting that there is significant broadening of the quadrupolar interaction

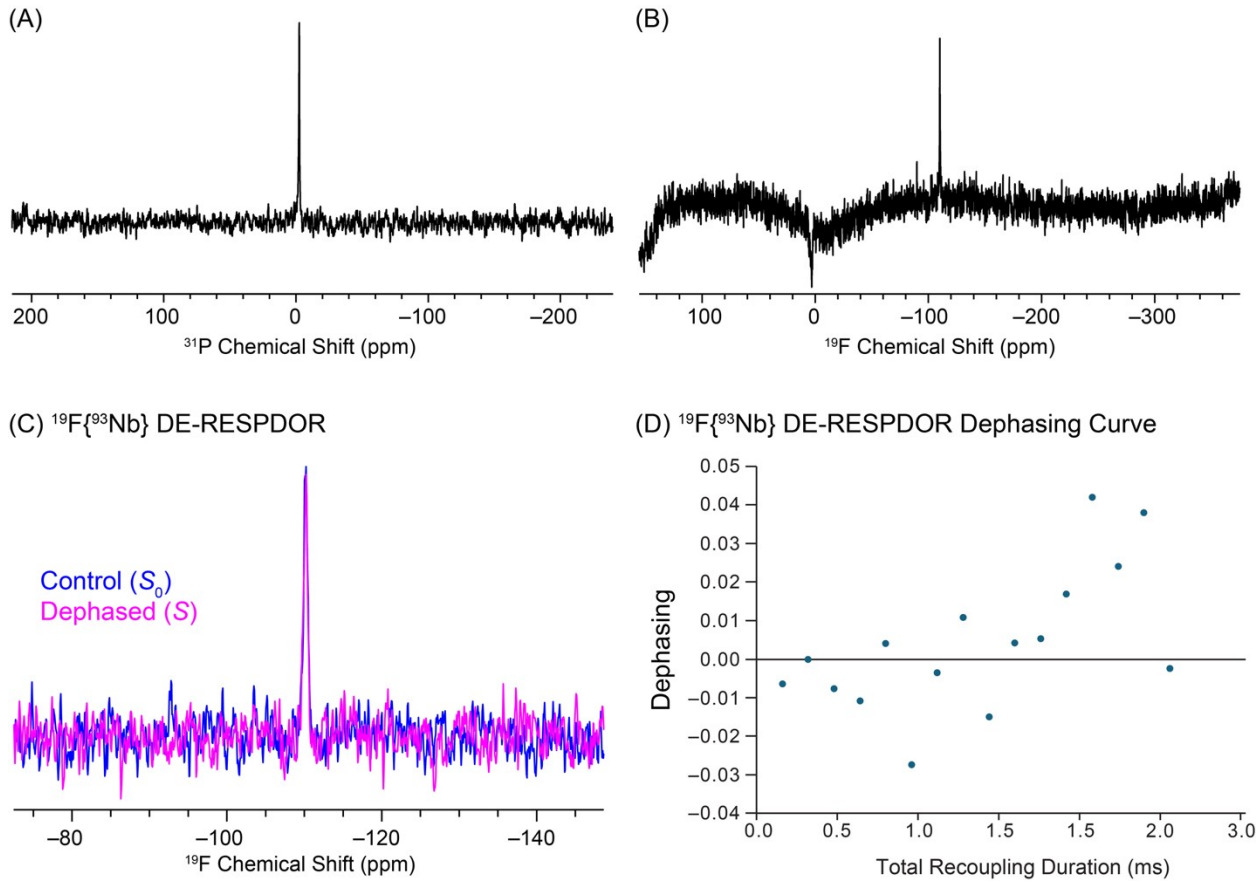

Figure S13. ^{31}P and ^{19}F MAS solid-state NMR spectra of the precipitate from the 50 mM Nb_{10}-DFP solution. The MAS frequency was 50 kHz. (A) ^{31}P MAS spin echo NMR spectrum showing a primary signal at –2.5 ppm. (B) MAS ^{19}F spin echo NMR shows a primary signal at –123 ppm. The baseline distortion and higher frequency signals around 0 ppm arise from the probe background. (C) ^{19}F{^{93}Nb} DE-RESPDOR control and dephased NMR spectra obtained with a total recoupling duration of 0.8 ms. The dephased spectrum was acquired by applying two 30 μs saturation pulses on ^{93}Nb with an approximate RF field of 90 kHz. No dephasing was observed. (D) Complete ^{19}F{^{93}Nb} DE-RESPDOR dephasing curve showing the normalized dephasing ($1–S/S_0$) as a function of the total recoupling duration. Within the uncertainty of the signal-to-noise ratio, no dephasing was observed.

Table S11 ^{31}P NMR chemical shift values of metal oxo cluster and DMMP reaction solution and their degradation periods.

Metal oxo cluster	Conversion (%) to MPA	Conversion period	Observed ^{31}P chemical shift values (ppm) and their assignments [39]
$\{Nb_6\}$ (50 mM)	21	6 hours	38.2 – DMMP; 28.2 – MP; 2.8 – inorganic phosphate
$\{Nb_6\}$ (5 mM)	9.9	20 days	38.5 – DMMP; 28.2 – MP; 8.4 - $PO(OH)(OCH_3)_2$
$\{Nb_{10}\}$ (50 mM)	0.6	11 days	38.2 – DMPP, 8.2 – $PO(OH)(OCH_3)_2$; 2.8 – inorganic phosphate
$\{Nb_{10}\}$ (5 mM)	1.5	20 days	38.5 – DMMP; 8.4 – $PO(OH)(OCH_3)_2$ 3.4 – inorganic phosphate
Li-$\{Nb_{24}\}$ (50 mM)	3	3 days	38.2 – DMMP; 28.2 – MP
Li-$\{Nb_{24}\}$ (5 mM)	2.9	21 days	38.5 – DMMP; 28.2 – MP; 8.4 – $PO(OH)(OCH_3)_2$
Cs-$\{Nb_{24}\}$ (50 mM)	1	4 days	38.2 – DMMP; 28.2 – MP
Cs-$\{Nb_{24}\}$ (5 mM)	4.2	21 days	38.5 – DMMP; 28.2 – MP; 8.4 – $PO(OH)(OCH_3)_2$
$\{Zr_4\}$ (50 mM)	0	n.a.	38.4 – DMMP
$\{Zr_4\}$ (5 mM)	0	n. a.	38.5 – DMMP
Control experiments:			
H_2O	0	n. a.	38.5 – DMMP
HCl	0	n. a.	38.5 – DMMP
CsOH	3.3	21 days	38.5 – DMMP; 28.2 – MP; 8.4 – $PO(OH)(OCH_3)_2$

DMMP studies.

Because DMMP and degradation products are soluble in IPA, this suggests selective, non-covalent association of phosphonates with the Nb-POMs. Interestingly, ^{31}P NMR of aqueous redissolved reaction precipitates shows a chemical shift at 28.2 ppm, consistent with association of the MP degradation product with Nb_6, Li-Nb_{24} and Cs-Nb_{24}. On the other hand, DMMP was absent, despite being far more abundant in these largely unreactive solutions (**figure S17**). Strong association of MP was also observed in both gas and liquid phase with $Cs_8[Nb_6O_{19}]$, inhibiting sustained reactivity.[37]

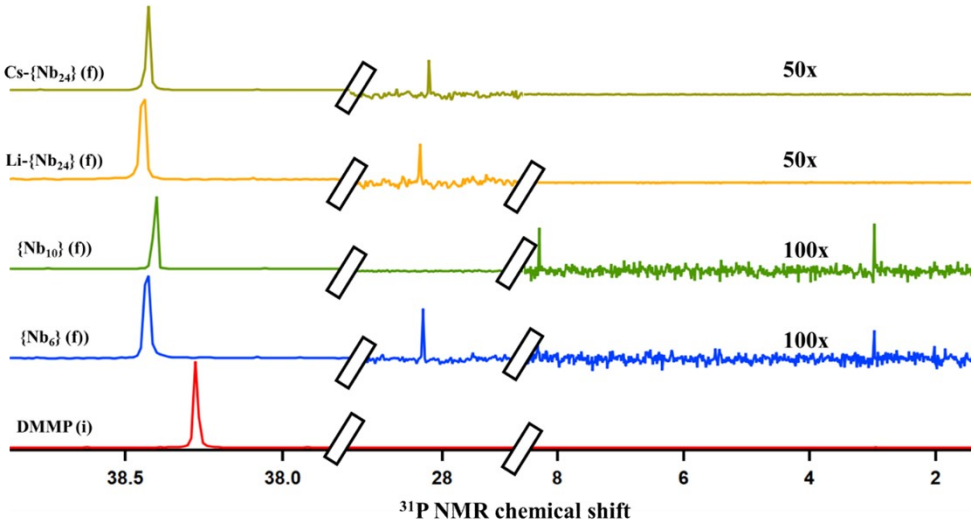

Figure S14 ^{31}P NMR chemical shift of PONbs and DMMP (50 mM – 50 mM) reaction solution.[39-41] (i= initial; f= final)

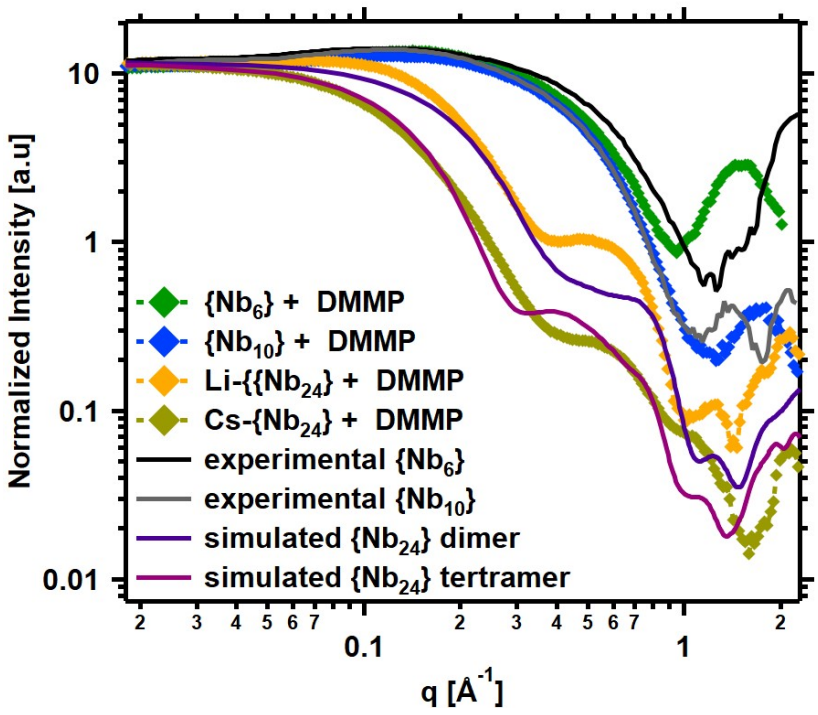

Figure S15 SAXS comparing metal-oxo cluster DMMP reaction solutions (50 mM – 50 mM). Intensity is normalized for ease of comparison, accounting for concentration differences in the reaction solutions, and the redissolved POM.

Table S12 EDX analysis of metals present in POM-DMMP reaction precipitates.

PONbs	at %P	at % Nb	PONb : P ratio
$\{Nb_6\}$ (50 mM)	10	90	1 : 0.3
$\{Nb_6\}$ (5 mM)	5	95	1 : 0.3
$\{Nb_{10}\}$ (50 mM)	8	92	1 : 0.9
$\{Nb_{10}\}$ (5 mM)	5	95	1 : 0.5
Li-$\{Nb_{24}\}$[1] (50 mM)	6	94	1 : 1.5
Li-$\{Nb_{24}\}$[1] (5 mM)	6	94	1 : 1.5
Cs-$\{Nb_{24}\}$ (50 mM)	6	60	1 : 2.4 (rest is Cs at 34%)
Cs-$\{Nb_{24}\}$ (5 mM)	4	59	1 : 1.7

[1]*Li not detectable by EDX*

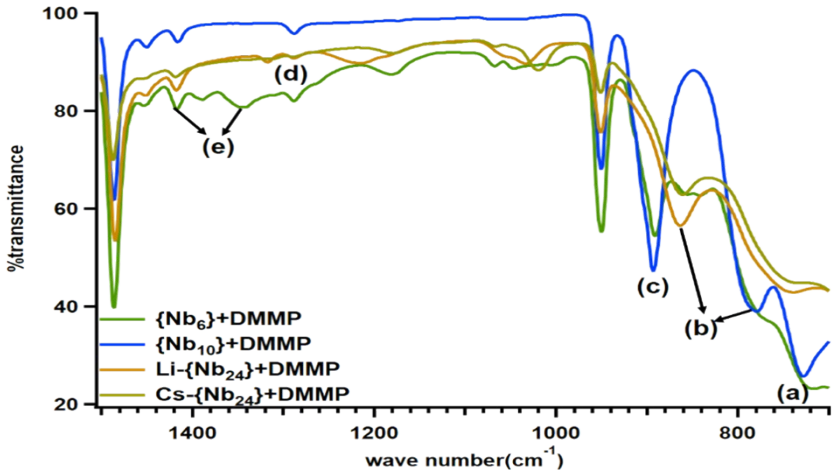

Figure S16 IR spectrum comparison among POMs DMMP a) ν(P=O) (713 cm^{-1}); b) $\nu(PO_2)$ (787 cm^{-1} and 818 cm^{-1}); c) $\rho(CH_3P)$ (911 cm^{-1}) d) ν(P=O) (1242 cm^{-1}) e) $\delta_a(CH_3P)$ (1313 cm^{-1} and 1420 cm^{-1}).[41]

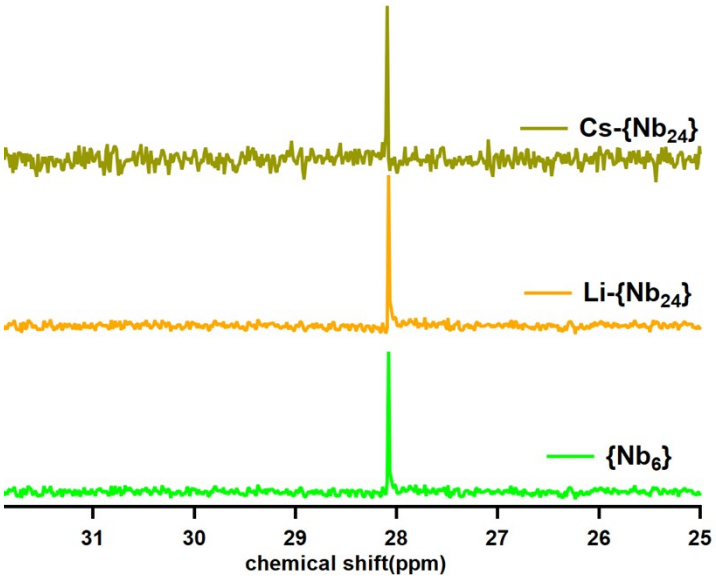

Figure S17 ^{31}P NMR on redissolved reaction precipitated of metal oxo cluster and DMMP.

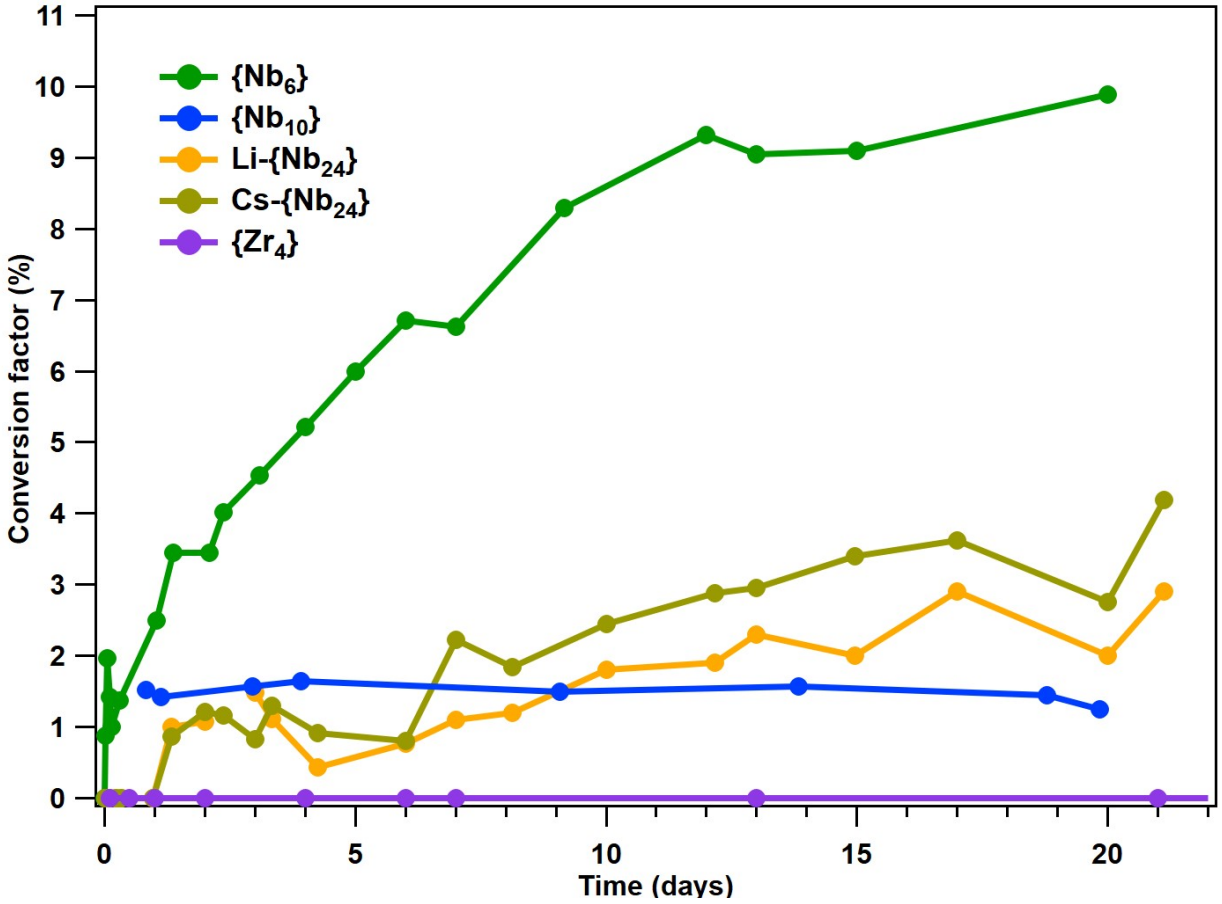

Figure S18 Comparison of DMMP degradation factors of the investigated metal-oxo clusters in the 5 mM-20 mM cluster-nerve agent reaction solutions obtained by ^{31}P NMR results.

Table S12 The obtained degradation degrees in 3-week degradation time-period in the metal-oxo cluster (5 mM) – DMMP (20 mM) reaction solutions.

System	Conversion factor (%)	Degradation period
$\{Nb_6\}$	9.9	20 days
$\{Nb_{10}\}$	1.5	20 days
Li-$\{Nb_{24}\}$	2.9	21 days
Cs-$\{Nb_{24}\}$	4.2	21 days
$\{Zr_4\}$	0	4 weeks
HCl	0	21 days
CsOH	3.3	15 days

References:

1. R. K. Harris, E. D. Becker, S. M. C. De Menezes, R. Goodfellow and P. Granger, *Pure Appl Chem*, 2001, **73**, 1795-1818.
2. F. H. Larsen, J. Skibsted, H. J. Jakobsen and N. C. Nielsen, *J Am Chem Soc*, 2000, **122**, 7080-7086.
3. A. Venkatesh, M. P. Hanrahan and A. J. Rossini, *Solid State Nucl Mag*, 2017, **84**, 171-181.
4. A. Brinkmann and A. P. M. Kentgens, *J Am Chem Soc*, 2006, **128**, 14758-14759.
5. B. A. Atterberry, S. L. Carnahan, Y. H. Chen, A. Venkatesh and A. J. Rossini, *J Magn Reson*, 2022, **336**.
6. N. E. Allen, S. K. Obendorf and J. Fan, *Rsc Adv*, 2016, **6**, 85985-85993.
7. C. J. Li, J. G. Guo, S. L. Cai, S. R. Zheng and W. G. Zhang, *Inorg Chem Commun*, 2016, **73**, 16-20.
8. S. Utamapanya, K. J. Klabunde and J. R. Schlup, *Chem Mater*, 1991, **3**, 175-181.
9. Y. X. Li and K. J. Klabunde, *Langmuir*, 1991, **7**, 1388-1393.
10. V. Stengl, V. Houskova, S. Bakardjieva, N. Murafa, M. Maríkova, F. Oplustil and T. Nemec, *Mater Charact*, 2010, **61**, 1080-1088.
11. M. K. Kinnan, W. R. Creasy, L. B. Fullmer, H. L. Schreuder-Gibson and M. Nyman, *Eur J Inorg Chem*, 2014, **2014**, 2361-2367.
12. W. W. Guo, H. J. Lv, K. P. Sullivan, W. O. Gordon, A. Balboa, G. W. Wagner, D. G. Musaev, J. Bacsa and C. L. Hill, *Angew Chem Int Edit*, 2016, **55**, 7403-7407.
13. J. Dong, J. F. Hu, Y. N. Chi, Z. G. Lin, B. Zou, S. Yang, C. L. Hill and C. W. Hu, *Angew Chem Int Edit*, 2017, **56**, 4473-4477.
14. J. Dong, H. J. Lv, X. R. Sun, Y. Wang, Y. M. Ni, B. Zou, N. Zhang, A. X. Yin, Y. N. Chi and C. W. Hu, *Chem-Eur J*, 2018, **24**, 19208-19215.
15. Y. Y. Liu, C. T. Buru, A. J. Howarth, J. J. Mahle, J. H. Buchanan, J. B. DeCoste, J. T. Hupp and O. K. Farha, *J Mater Chem A*, 2016, **4**, 13809-13813.
16. E. López-Maya, C. Montoro, L. M. Rodríguez-Albelo, S. D. A. Cervantes, A. A. Lozano-Pérez, J. L. Cenís, E. Barea and J. A. R. Navarro, *Angew Chem Int Edit*, 2015, **54**, 6790-6794.
17. J. C. Jiang, F. Gándara, Y. B. Zhang, K. Na, O. M. Yaghi and W. G. Klemperer, *J Am Chem Soc*, 2014, **136**, 12844-12847.
18. M. J. Katz, Z. J. Brown, Y. J. Colón, P. W. Siu, K. A. Scheidt, R. Q. Snurr, J. T. Hupp and O. K. Farha, *Chem Commun*, 2013, **49**, 9449-9451.
19. P. Li, S. Y. Moon, M. A. Guelta, S. P. Harvey, J. T. Hupp and O. K. Farha, *J Am Chem Soc*, 2016, **138**, 8052-8055.
20. Y. Y. Liu, A. J. Howarth, J. T. Hupp and O. K. Farha, *Angew Chem Int Edit*, 2015, **54**, 9001-9005.
21. R. Zboril, M. Andrle, F. Oplustil, L. Machala, J. Tucek, J. Filip, Z. Marusak and V. K. Sharma, *J Hazard Mater*, 2012, **211**, 126-130.
22. G. W. Wagner, L. R. Procell and S. Munavalli, *J Phys Chem C*, 2007, **111**, 17564-17569.
23. T. J. Bandosz, M. Laskoski, J. Mahle, G. Mogilevsky, G. W. Peterson, J. A. Rossin and G. W. Wagner, *J Phys Chem C*, 2012, **116**, 11606-11614.
24. B. Singh, T. H. Mahato, A. K. Srivastava, G. K. Prasad, K. Ganesan, R. Vijayaraghavan and R. Jain, *J Hazard Mater*, 2011, **190**, 1053-1057.
25. P. Janos, P. Kuran, M. Kormunda, V. Stengl, T. M. Grygar, M. Dosek, M. Stastny, J. Ederer, V. Pilarova and L. Vrtoch, *J Rare Earth*, 2014, **32**, 360-370.

26. G. K. Prasad, T. H. Mahato, P. Pandey, B. Singh, M. V. S. Suryanarayana, A. Saxena and K. Shekhar, *Micropor Mesopor Mat*, 2007, **106**, 256-261.
27. G. K. Prasad, P. V. R. K. Ramacharyulu, K. Batra, B. Singh, A. R. Srivastava, K. Ganesan and R. Vijayaraghavan, *J Hazard Mater*, 2010, **183**, 847-852.
28. J. Dong, D. Zhang, P. X. Zhang, C. P. Liu, J. Li, J. Bai, Y. N. Chi and C. W. Hu, *Coordin Chem Rev*, 2024, **517**.
29. L. Bromberg, Y. Klichko, E. P. Chang, S. Speakman, C. M. Straut, E. Wilusz and T. A. Hatton, *Acs Appl Mater Inter*, 2012, **4**, 4595-4602.
30. H. R. Tang, Z. X. Cheng, H. Y. Zhu, G. M. Zuo and M. Zhang, *Appl Catal B-Environ*, 2008, **79**, 323-333.
31. A. Mattsson, C. Lejon, V. Stengl, S. Bakardjieva, F. Oplustil, P. O. Andersson and L. Österlund, *Appl Catal B-Environ*, 2009, **92**, 401-410.
32. G. K. Prasad, *J Sci Ind Res India*, 2009, **68**, 379-384.
33. D. A. Giannakoudakis, F. Pearsall, M. Florent, J. Lombardi, S. O'Brien and T. J. Bandosz, *J Colloid Interf Sci*, 2018, **531**, 233-244.
34. P. V. Korake, R. S. Dhabbe, A. N. Kadam, Y. B. Gaikwad and K. M. Garadkar, *J Photoch Photobio B*, 2014, **130**, 11-19.
35. S. R. Kline, *J Appl Crystallogr*, 2006, **39**, 895-900.
36. a)K. E. Johnston, J. M. Griffin, R. I. Walton, D. M. Dawson, P. Lightfoot and S. E. Ashbrook, *Phys Chem Chem Phys*, 2011, **13**, 7565-7576; b)M. Tansho, A. Goto, S. Ohki, Y. Mogami, Y. Yasui, Y. Sakuda, K. Fujii, T. Iijima and M. Yashima, *J Phys Chem C*, 2024, **128**, 19679-19687; c)A. Flambard, L. Montagne, L. Delevoye and S. Steuernagel, *Solid State Nucl Mag*, 2007, **32**, 34-43; d)O. B. Lapina, D. F. Khabibulin, K. V. Romanenko, Z. H. Gan, M. G. Zuev, V. N. Krasil'nikov and V. E. Fedorov, *Solid State Nucl Mag*, 2005, **28**, 204-224.
37. Q. Wang, R. Chapleski, A. M. Plonka, W. O. Gordon, W. W. Guo, T. D. Nguyen-Phan, C. H. Sharp, N. S. Marinkovic, S. D. Senanayake, J. R. Morris, C. L. Hill, D. Troya and A. I. Frenkel, *Sci Rep-Uk*, 2017, **7**, 773.